Designable Dirac Point Voltage of Graphene by Mechanical Bending Ferroelectric gate of Graphene Field Effect Transistor and Its Multifunctional Application

Journal:	*Materials Horizons*
Manuscript ID	MH-COM-11-2018-001499
Article Type:	Communication
Date Submitted by the Author:	23-Nov-2018
Complete List of Authors:	Hu, Guangliang; Xi'an Jiaotong University Wu, Jingying; Xi'an Jiaotong University Ma, Chunrui; Xi'an Jiaotong University, Liang, Zhongshuai; Xi'an Jiaotong University Liu, Weihua; Department of Microelectronics, Xi'an Jiaotong University Liu, Ming; Xi'an Jiaotong University, School of Electronic and Information Engineering Wu, Judy; University of Kansas, Department of Physics and Astronomy Jia, Chun-Lin; School of Microelectronics; Peter Grünberg Institute and Ernst Ruska Center for Microscopy and Spectroscopy with Electrons

SCHOLARONE™
Manuscripts

Conceptual Insights

Graphene has been widely used in various electronic devices and controlling the doping state or Dirac point voltage (V_{Dirac}) of graphene is essential for its practical applications. Different from traditional methods to modulate the doping in graphene, such as UV radiation in different gas environments, absorption of ionic liquid/ionic gel or gas molecules, here, we proposed a new method by applying mechanical bending stress on an all-inorganic flexible graphene-field effect transistor (GFET). Compared to other methods, the mechanical stress/strain designed graphene doping has three advantages: (i) it does not involve the absorption from secondary substances like gas molecules or ionic liquids; (ii) it is recoverable without any change on graphene; (iii) the doping operation is simple and reliable. The GFET with ferroelectric gate ($Pb_{0.92}La_{0.08}Zr_{0.52}Ti_{0.48}O_3$ thin film) exhibits a linear shift of Dirac point with increasing the bending stress duo to the flexoelectric effect of ferroelectric gate. These phenomena indicate that it can be used to both tune the graphene doping state through adjusting curvature and detect bending curvature by monitoring the variability of its V_{Dirac}. This makes it enormously useful in the flexible electronic devices and flexible deformation sensors.

Journal Name

COMMUNICATION

Designable Dirac Point Voltage of Graphene by Mechanical Bending Ferroelectric gate of Graphene Field Effect Transistor and Its Multifunctional Application [†]

Guangliang Hu[ab], Jingying Wu[b], Chunrui Ma*[a], Zhongshuai Liang[b], Weihua Liu[b], Ming Liu[b], Judy Z. Wu[c], Chun-Lin Jia[bd]

Control of Dirac point voltage of graphene is essential for various practical applications of graphene. Here, a designable doping effect is achieved in flexible graphene field effect transistors (GFETs) by mechanical bending stress. By gradually increasing the bending strain (the decrease of upward/downward bending radius), the Dirac point (V_{Dirac}) linearly shifts to left/right, which is induced by the flexoelectric effect of the ferroelectric $Pb_{0.92}La_{0.08}Zr_{0.52}Ti_{0.48}O_3$ (PLZT) gate. In additional, a superior mechanical antifatigue character is obtained in the flexible GFETs, and the doping effect is recoverable. The sensitive characteristics to strain and high bending stability not only offers an easy, controllable and nonintrusive method to obtain a specific doping graphene for flexible electric device, but also promise the flexible ferroelectric PLZT-gated GFETs enormous potential applications as wearable sensors.

1. Introduction

Graphene, a monolayered carbon material with a hexagonal structure, has been considered as a promising material for high-performance nanoelectronics due to its superior chemical stability, high electron mobility, mechanical flexibility and high transmittance[1-3]. Especially, the ambipolar characteristics of graphene based on field effect transistors (GFETs) make them highly competitive with the present electronic devices, since the graphene can behave as n-type or p-type by doping. Until now, great efforts have been performed to modulate the doping in graphene, such as UV radiation in different gas environments, absorption of ionic liquid/ionic gel or gas molecules[4-6]. Actually, graphene doping by these methods are realized through surface-transfer doping, which involves electron exchange between graphene and dopants. It is known that a mechanical stress/strain can break centrosymmetry and hence generate a spontaneous electrical polarization (electric charge) in a dielectric material. Therefore, graphene can be tuned by applying a mechanical stress/strain to the gate (dielectric material) of flexible GFETs in principle. Compared to other methods, the mechanical stress/strain tunable has three advantages: (i) it does not involve the absorption from secondary substances like gas molecules or ionic liquids; (ii) it is recoverable without any change on graphene; (iii) the doping operation is simple and reliable. Based on the above advantages, the mechanical stress/strain is ideally suitable for tuning graphene doping. Unfortunately, the research of mechanical stress/strain tunable GFETs is lacking presently.

Moreover, the rapidly increasing demands for human-machine interfacing have driven flexible devices become one of the greatest technological and societal challenges nowadays[7-12]. Flexible thin film is a key component of wearable sensors. Recently, some inorganic functional oxide thin films, such as $CuFe_2O_4$ and $LiFe_5O_8$, have been made flexible by directly fabricating the desired thin film on flexible Mica substrate or transferring the desired thin film from rigid substrates to flexible substrate through etching a buffer layer between the desired thin film and rigid substrate[13, 14]. It is known that the inorganic ferroelectric thin films as the gate of GFETs can significantly low down the operating voltage, compared with the conventional gate materials (SiO_2/Al_2O_3) or the organic flexible ferroelectric gate. For example, the popular organic ferroelectric gate made of poly((vinylidenefluoride-co-trifluoroethylene) (P(VDF-TrFE)) requires operating voltage of at least ±5 V, but typically at ±40 V. While these are among the lowest reported on the organic ferroelectric gates, the operating voltage on organic gates is significant greater than that for the inorganic ferroelectric gates, such as $Pb_{0.92}La_{0.08}Zr_{0.52}Ti_{0.48}O_3$ (PLZT) or $PbZr_{0.2}Ti_{0.8}O_3$ with operation voltage typically less than ±2 V[12, 15-17]. In addition, GFETs provide a unique platform to design various sensors since the conductance of GFET channel is sensitive to

interfacial electrical charges with high bipolar electrical susceptibility[1, 18]. Using PLZT-gated GFETs, we have demonstrated detection of the dynamic self-assembly of monolayer molecular ions on graphene[19], and the high sensitivity is anticipated from the high gate efficiency of the ferroelectric PLZT gate[6, 16]. Herein, we design an all-inorganic flexible ferroelectric-gated GFET based on the PLZT gate on Fluorophlogopite (F-Mica) substrate. Remarkably, the GFET Dirac point (V_{Dirac}) can be tuned by mechanical bending linearly. Based on the change of the Dirac point, this kind flexible GFETs have broad application prospect. Through the tuning of curvature, we can obtain a specific Dirac point that we need, which can be used in the flexible electronic or optoelectronic devices requiring a controllable doping graphene. Furthermore, by monitoring the variability of I_D (source-drain current)-V_G (gate voltage) characteristics, the curvature variation can be detected, which can be used in field of flexible deformation sensors, such as the motion of soft robotics and human.

2. Results

Multilayer films of PLZT/La$_{0.67}$Sr$_{0.33}$MnO$_3$/SrTiO$_3$ (PLZT/LSMO/STO) were fabricated by Pulse Laser Deposition (PLD) on F-mica. The crystallinity of the films has been characterized using x-ray diffraction (XRD) as shown in Fig. S1(a). It can be seen only (111) peak can be seen for both STO buffer layer and LSMO electrode layer on (00l) F-mica substrate. Combined with the φ scans performed around from the (002) reflections of the LSMO/STO and the (202) reflections of the F-mica substrate shown in Fig. S1(b), the LSMO/STO is most probably form an epitaxial relationship of (111)$_{LSMO}$//(111)$_{STO}$//(001)$_{F\text{-mica}}$ and [1$\bar{1}$0]$_{LSMO}$//[1$\bar{1}$0]$_{STO}$//[010]$_{F\text{-mica}}$. The PLZT film fabricated on LSMO/STO is also highly oriented. Only a minor peak of (101) was detectable besides the main (111) PLZT peak.

A structure of the flexible GFET was designed and its fabrication process is schematically shown in Fig. 1(a). The LSMO film layer is used as the back-gate electrode and the Pt layer parts are used as the source drain electrode. The GFET channel is about 30 μm in length and 50 μm in width. Fig. 1(b) shows the Raman spectrum of the graphene channel. The intensity of the 2D peak is around twice of that of G peak, which is anticipated on the single-layer graphene. The GFET sample was annealed in vacuum below 10^{-6} Pa for about 24 hours before the electrical transport measurement to remove the residual adsorbates attached to the GFET channel in the GFET fabrication process[16]. The source-drain current (I_D) on a representative PLZT-gated GFET (black) is depicted in Fig. 1c as function of gate voltage V_G with a fixed source-drain bias V_D=20 mV. The leakage current through the PLZT gate (blue) is less than 50 nA as shown in the same figure. The Dirac point V_{Dirac} is 0.72 V. The positive V_{Dirac} indicates the graphene is p-

doped, which is attributed to the polarization of PLZT ferroelectric gate[16, 20].

The differential transconductance g_m of the PLZT-gated GFET can be obtained from the I_D-V_G characteristic by the formula:

$$g_m = dI_D/dV_G. \quad (1)$$

It is shown in Fig. 1(d) in the V_G range of ±2 V. The field effect mobility of holes and electrons can be calculated from the peak transconductance using the formula[21, 22]:

$$\mu = g_m L/(W C_G V_D). \quad (2)$$

Where, L is the channel length, W is the channel width, V_D is the drain voltage and C_G is the specific capacitance of gate. The calculated field effect mobility of holes and electrons are $\mu_{h,B}$=54.8 cm^2·V^{-1}·s^{-1} and $\mu_{e,B}$=58.7 cm^2·V^{-1}·s^{-1}, respectively, which are comparable to the results of our previous work for the PLZT-gated GFET on Nb:STO substrate[18]. The reason for the low graphene mobility is complex, the defects of graphene (such as cracks or folding by transfer procedure), the screening effect at the graphene/PLZT interface and nanoscale scattering mechanisms may play an important role[16, 22, 23].

In order to investigate the tuning effect by mechanical strain on the transfer characteristic of GFET with the PLZT gate, the F-Mica substrate was mechanically exfoliated down to few tens of micrometers to obtain a good flexibility and then the GFET device was transferred on a Polyimide tape for bending test. Firstly, the strain is introduced by upward bending. The strain was changed by bending the Polyimide tape at various curvature radii of 12 mm, 10 mm, 8 mm and 6 mm, respectively. The I_D-V_G characteristics of the flexible PLZT-gated GFET at different curvature radii are shown in Fig. 2(a) and the inset is a photo of the bending measurement. Despite a little change in I_D at the V_{Dirac}, which may be caused by the effect of air atmosphere, the mobilities of hole and electron are almost the same with increasing bending ratio from no bending to 6 mm bending radius. The V_{Dirac} exhibits a consistent left shift from 0.72 V in flat state to 0.4 V at the 6 mm bending radius. Interestingly, the V_{Dirac} shift is almost linear with the decreasing bending radius as shown in Fig. 2(b) (fitted by the red line). Secondly, a strain is introduced by downward bending. As shown in Fig. S2(a), a similar linear shift of I_D-V_{BG} curves with decreasing bending radius can be obtained. However, the V_{Dirac} shifts toward positive value. The details are showed in Fig. 2(c), a linear increase of V_{Dirac} can be seen as bending radius decreases, and the total right shift is about 0.31 V. In fact, this response is highly reproducible, suggesting the all-inorganic flexible GFET exhibits excellent flexural fatigue as shown in Fig. S2(b). Basically, the I_D-V_G curves of the GFET bending cycle between 1 and 1000 under bending radius (downward bending) of 6 mm coincide well. The V_{Dirac} of these curves are extracted and summarized in Fig. 2(d). Although the V_{Dirac} shows a slight increase of 0.04 V when the bending cycling is above 500, no further changes are observed, suggesting that the PLZT-gated flexible GFET has a

stable flexural fatigue characteristic. The similar flexural fatigue property for upward bending can be seen in Fig. S3.

The linear shift of V_{Dirac} with the increasing bending curvature (or decreasing bending radius) can be understood based on two factors. One is the GFET channel and the other one is the characteristics of the gate, in response to the bending. S.I. Kundalwal *et. al.*stated [24] the magnitude of the dipole moment per atom presents a sharp linear decrease (from 0.2 D to 0.03 D) with increasing the radius of curvature from 11.8 Å to 15.2 Å. So, when the radius of curvature up to millimeter level, as that in our case, the magnitude of the dipole moment should be too small to be ignored. Therefore, here we focus the investigation on curvature-induced polarization of PLZT ferroelectric gate. The ferroelectric properties of the PLZT with LSMO as bottom electrode and Pt as the top electrode are shown in Fig. 3. Fig. 3(a) depicts the polarization-voltage (*P-V*) hysteresis loops at selected maximum applied voltages in the range of 2~20 V. It can be seen that the coercive voltage V_c+ and Vc- are asymmetric, especially at high voltage. This is caused by the build-in electric field at the interface between electrode (Pt/LSMO) and PLZT thin films.[25] The V_c+ is less than 2 V, meaning 2 V gate voltage is adequate to induce sufficient charge density in the GFET channel for observation of electric dipole alignment and switch in the ferroelectric PLZT gate as the polarization of PLZT induced charge in GFET channel can change the doping state of the graphene. Fig. 3(b) depicts the leakage current density measured as a function of applied voltage, which shows a maximum value of around 1×10^{-7} A/cm^2 at ±2 V. The low leakage current density observed suggests that the PLZT films have desired high resistivity for the gate dielectric applications. Fig. 3(c) shows the *P-V* characteristics of PLZT film at the maximum voltage of 2 V under the various upward bending state with curvature radii of 12 mm, 10 mm, 8 mm and 6 mm. It can be seen a upward shift of the *P-V* loops with increasing the upward bending curvature. Fig.3(d) and (e) show the V_c and P_r of these curves, respectively. It can be seen that both V_c+ and V_c- linearly decrease with increasing the upward bending curvature. The total shift of V_c+ and V_c- are about 0.19 V and 0.16 V, respectively. The P_r+ and P_r- increase with increasing the upward bending curvature and the total shift of P_r+ and P_r- are about 0.21 μC/cm^2 and 0.22 μC/cm^2, respectively. However, for downward bending, the *P-V* loops have an opposite change, as shown in Fig. 3(f). V_c+ and V_c- increase (Fig.3(g)) and P_r+ and P_r- decrease (Fig.3(h)) with increasing the downward bending curvature. The total shift of V_c+ and V_c- is same, abround 0.13 V. While, the total shift of P_r+ and P_r- are about 0.22 μC/cm^2 and 0.20 μC/cm^2, respectively. The total polarization of PLZT can be given by the constitutive equation:[26]

$$P = \chi E + \mu \frac{\partial u}{\partial x}. \tag{3}$$

The first term describes the dielectric response with the clamped dielectric susceptibility χ, and the second term describes the flexoelectric response with the flexoelectric coefficient μ. *E* and $\partial u/\partial x$ are applied electric field and strain gradient, respectively. As shown in Fig. 4(a), the polarization (P_B) induced by the upward bending is up (middle figure), while the polarization induced by the downward bending is down (right figure). From the Equ. 3 and the strain gradient calculation shown in Fig. S4, it can be derived that the polarization induced by strain gradient increases as the bending curvature increase[26-28]. For upward bending case (Fig.4(b)) when a positive voltage (*V*+) applied to the bottom electrode, the direction of polarization induced by applied electric field (P_E) is parallel to P_B. When a negative voltage (*V*-) applied to the bottom electrode, the direction of P_E is antiparallel to P_B. Therefore, the *P-V* loops will take a upward shift, which is consistant with the measured *P-V* loops (Fig. 3(c)). The downward bending (Fig.4(c)) generate an opposite behavior, that is the polarization induced by *V*+ is antiparallel to P_B , and the polarization induced by *V*- is parallel to P_B, and will make the *P-V* loops shift downward (Fig. 3(e)). The upward polarization generated by the upward bending contributes positive charges at the surface of the PLZT thin film. For compensation of the positive charges, negative charges are accumulated in graphene, , as depicted in Fig. 4(d), leading to a negative-charge-doping effect and a left shift of the V_{Dirac}. With increasing the bending curvature, more positive charges are generated and hence induce the V_{Dirac} left shift further. Conversely, the polarization induced by downward bending results in a positive-charge-doping effect in graphene, as shown in Fig. 4(e), and a right shift of V_{Dirac}.

In order to quantitatively analyze the effect of the mechanical bending on the doping of graphene, we calculated the change of charge carrier (Δ*Q*) in graphene under bending state. As we known, the charge carrier change is related to the Dirac point shift (ΔV_{Dirac}) by Δ$Q=C_g·$ΔV_{Dirac}, where C_g is back gate capacitance. From Fig. 2, it can be seen that the total change of V_{Dirac} under upward bending and downward bending are about 0.32 V and 0.31 V ,respectively, when the device is bent from ∞ to 6 mm bending radius. As shown in Fig. S5, the capacitance of back-gate is 0.6 uF/cm^2, which leads to the charge carrier change of around 0.192 μC/cm^2 and 0.186 μC/cm^2 in graphene for upward bending and downward bending, respectively. They are comparable to the polarization change of ΔP_r, as shown in Fig. 3(d) and Fig. 3(f). Based on the experiment results and above discussions, the change of polarization of PLZT and V_{Dirac} of GFET is mainly caused by the flexoelectric effect of PLZT thin film. Moreover, the good characteristic in flexural fatigue of PLZT thin film, as shown in Fig. S6, provides the stability for the flexible GFET device. These phenomena suggest that the mechanical bending can be used to tune the graphene doping state according to the change of the I_D-V_G characteristics (V_{Dirac}), which provide great opportunities for wearable mechanics-electronic sensors and flexible electronic devices, as shown in Fig. 5. By monitoring the change of I_D-V_G characteristics (Dirac point voltage), the curvature variation can be detected (process 1 in Fig. 5), which

can be used in the field of flexible deformation sensor to detect the mechanical movement state, such as the human or robot bending action. On the other hand, we can get specific graphene doping state (Dirac point voltage) that we need through tuning the mechanical bending stress (curvature), which can be used in the flexible GFETs and other flexible electronic devices (process 2 in Fig. 5).

3.   Conclusions

In summary, a tunable Dirac point voltage have been achieved in an all-inorganic flexible GFET by mechanical bending stress. The I_D-V_G characteristics exhibits a continuous change in the Dirac point voltage under the mechanical strain (both upward and downward bending). It is exciting that the change of Dirac point voltage with the mechanical bending strain is linear resulting from the fact that the flexoelectric effect of ferroelectric PLZT gate generates additional positive (negative) charges at the surface of PLZT thin film with upward (downward) mechanical bending and induces electron-doping (hole-doping) effect into graphene. This provides great opportunities for the wearable mechanical sensors and flexible electric devices requiring a specific doping graphene. What's more important, the PLZT-gated GFET devices exhibit excellent stability against flexural fatigue with negligible degradation after 1000 bending cycles. Therefore, the flexible all-inorganic GFET device are promising for widely applications in flexible sensing systems.

4.   Experimental Method

Fabrication of thin Film

A buffer layer of ~30 nm $SrTiO_3$ (STO) was first epitaxially growth on the F-mica substrate by KrF excimer pulsed laser deposition system with a wavelength 248 nm at 800 °C and 50 mTorr oxygen pressure. On the buffer layer the electrode LSMO (about 45 nm) was epitaxially grown at 700 °C in oxygen atmosphere with a pressure of 50 mTorr. Then, the LSMO/STO double layers were annealed at 700 °C for 15 mins under 400 Torr oxygen atmospheres and cooled down to room temperature at the rate of 5 °C/min. Afterwards, a PLZT thin film was deposited on the LSMO/STO films with a thickness of 500 nm. The PLZT growth condition was selected under an oxygen pressure of 150 mTorr at 650 °C. After the growth, the PLZT thin films were annealed at the growth temperature for 15 min in pure oxygen (350 Torr) and then naturally cooled down to room temperature. The laser energy density was about 2.0 $J·cm^{-2}$ with laser repetition rate of 5 Hz for LSMO and PLZT film and 3 Hz for STO film, respectively.

Graphene Transfer

A layer of Poly-methyl methacrylate (PMMA) was spin-coated on a commercial graphene/Cu sheet with typically 1×1 cm^2 in dimension (Muke Nano, Nanjing) and baked in air at 60 °C for 10 mins. Before removing the Cu sheet by immersing the graphene sample into a copper etchant (solution of ammonium persulfate stabilization), it was cut into a small

sheet of 0.2×0.6 cm^2 in dimension to expose the edge of the copper for etching. The PMMA/graphene was rinsed with deionized (DI) water for multiple times after the copper was fully dissolved. The graphene sample was then transferred onto the PLZT with a pre-fabricated Pt source and drain electrodes and baked in air at 150 °C for one hour to eliminate moisture. The PMMA on graphene was removed by acetone, then the sample was rinsed by isopropyl alcohol to remove residues on the graphene surface.

Characterization

The crystallinity of the PLZT, STO and LSMO thin films was characterized using a high-resolution X-ray diffraction system (HRXRD, PANalytical X'Pert MRD). For measurement of properties, Pt quadrates with 200 μm in length and 70 nm in thickness were deposited on the PLZT samples by sputtering through a shadow mask. The P-E loops were measured by TF Analyzer 2000E with FE-Module at a frequency of 1 kHz. The structure of graphene was characterized by Laser Raman Spectrometer (LabRAM HR Evolution, HORIBA Scientific), and the instrument is equipped with a standard 633 and 532 nm laser. For the electrical transport property measurement in air, a layer of PMMA was casted on the graphene channel for passivation. In addition, vacuum cleaning (< 2×10^{-6} Torr) was applied to the GFET samples for further removal of the residues on graphene channel[16, 29]. The transport properties of the flexible ferroelectric-gated GFETs were characterized using an Agilent B4155C semiconductor analyzer. Half-cylinders with different diameter were used for the bending measurement.

Conflicts of interest

There are no conflicts to declare.

Acknowledgements

Notes and references

1   N. O. Weiss, H. Zhou, L. Liao, Y. Liu, S. Jiang, Y. Huang, X. Duan, *Adv. Mater.* 2012, **24**, 5782-5825.
2   A. K. Geim, Science 2009, **324**, 1530-1534.
3   C. Lee, X. D. Wei, J. W. Kysar, J. Hone, *Science* 2008, **321**, 385-388.
4   A. Inaba, K. Yoo, Y. Takei, K. Matsumoto, I. Shimoyama, *Sens. Actuators, B* 2014, **195**, 15-21.
5   L. P. Wu, L. Qin, Y. Zhang, M. Alamri, M. G. Gong, W.

Zhang, D. Zhang, W. L. Chan, J. Z. Wu, *ACS Appl. Mater. Interfaces* 2018, **10**, 12824-12830.

6   C. Ma, R. Lu, G. Hu, J. Han, M. Liu, J. Li, J. Wu, *ACS Appl. Mater. Interfaces* 2017, **9**, 4244-4252.

7   H. Yu, C. C. Chung, N. Shewmon, S. Ho, J. H. Carpenter, R. Larrabee, T. L. Sun, J. L. Jones, H. Ade, B. T. O'Connor, F. So, *Adv. Funct. Mater.* 2017, **27**, 1700461.

8   G. Schwartz, B. C. K. Tee, J. G. Mei, A. L. Appleton, D. H. Kim, H. L. Wang, Z. N. Bao, *Nat. Commun.* 2013, **4**, 1859.

9   T. Q. Trung, N. T. Tien, D. Kim, M. Jang, O. J. Yoon, N. E. Lee, *Adv. Funct. Mater.* 2014, **24**, 117-124.

10   M. Song, J. Seo, H. Kim, Y. Kim, *Sci. Rep.* 2017, **7**, 2630.

11   X. H. Wu, Y. Ma, G. Q. Zhang, Y. L. Chu, J. Du, Y. Zhang, Z. Li, Y. R. Duan, Z. Y. Fan, J. Huang, *Adv. Funct. Mater.* 2015, **25**, 2138-2146.

12   X. D. Wang, M. H. Tang, Y. Chen, G. J. Wu, H. Huang, X. L. Zhao, B. B. Tian, J. L. Wang, S. Sun, H. Shen, T. Lin, J. L. Sun, X. J. Meng, J. H. Chu, *Opt. Quantum Electron.* 2016, **48**, 345 .

13   W. L. Liu, M. Liu, R. Ma, R. Y. Zhang, W. Q. Zhang, D. P. Yu, Q. Wang, J. N. Wang, H. Wang, *Adv. Funct. Mater.* 2018, **28**, 1705928.

14   L. K. Shen, L. Wu, Q. Sheng, C. R. Ma, Y. Zhang, L. Lu, J. Ma, J. Ma, J. H. Bian, Y. D. Yang, A. P. Chen, X. L. Lu, M. Liu, H. Wang, C. L. Jia, *Adv. Mater.* 2017, **29**, 1702411.

15   N. H. Van, J. H. Lee, D. Whang, D. Kang, *Nano-Micro Lett.* 2015, **7**, 35-41.

16   C. Ma, Y. Gong, R. Lu, E. Brown, B. Ma, J. Li, J. Wu, *Nanoscale* 2015, **7**, 18489-18497.

17   C. Baeumer, S. P. Rogers, R. J. Xu, L. W. Martin, M. Shim, *Nano Lett.* 2013, **13**, 1693-1698.

18   G. L. Hu, G. P. Pandey, Q. F. Liu, R. S. Anaredy, C. R. Ma, M. Liu, J. Li, S. K. Shaw, J. Wu, *ACS Appl. Mater. Interfaces* 2017, **9**, 35437-35443.

19   G. Hu, C. Ma, W. Wei, Z. Sun, L. Lu, S.-B. Mi, M. Liu, B. Ma, J. Wu, C.-l. Jia, *Appl. Phys. Lett.* 2016, **109**, 193904.

20   A. Di Bartolomeo, F. Giubileo, F. Romeo, P. Sabatino, G. Carapella, L. Iemmo, T. Schroeder, G. Lupina, *Nanotechnology* 2015, **26**, 475202.

21   S. C. Sun, J. D. Plummer, *Ieee J. Solid-State Circuits* 1980, **15**, 562-573.

22   G. Fisichella, S. Lo Verso, S. Di Marco, V. Vinciguerra, E. Schiliro, S. Di Franco, R. Lo Nigro, F. Roccaforte, A. Zurutuza, A. Centeno, S. Ravesi, F. Giannazzo, *Beilstein J. Nanotechnol.* 2017, **8**, 467-474.

23   F. Giannazzo, S. Sonde, R. Lo Nigro, E. Rimini, V. Raineri, *Nano Lett.* 2011, **11**, 4612-4618.

24   S. I. Kundalwal, S. A. Meguid, G. J. Weng, *Carbon* 2017, **117**, 462-472.

25   K. Abe, N. Yanase, T. Yasumoto, T. Kawakubo, *J. Appl. Phys.* 2002, 91, 323-330.

26   P. Zubko, G. Catalan, A. K. Tagantsev, *Annu. Rev. Mater. Res.* 2013, **43**, 387-421.

27   F. Ahmadpoor, P. Sharma, *Nanoscale* 2015, **7**, 16555-16570.

28   Q. Deng, M. Kammoun, A. Erturk, P. Sharma, *Int. J. Solids Struct.* 2014, **51**, 3218-3225.

29   R. T. Lu, J. W. Liu, H. F. Luo, V. Chikan, J. Z. Wu, *Sci. Rep.* 2016, **6**, 19161.

Table of Contents Entry
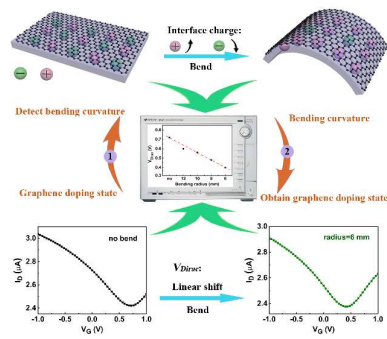
The linearly V_{Dirac} shift of the flexible GFET caused by flexoelectric effect of PLZT gate makes it enormously useful to both tune the graphene doping state and detect bending curvature.
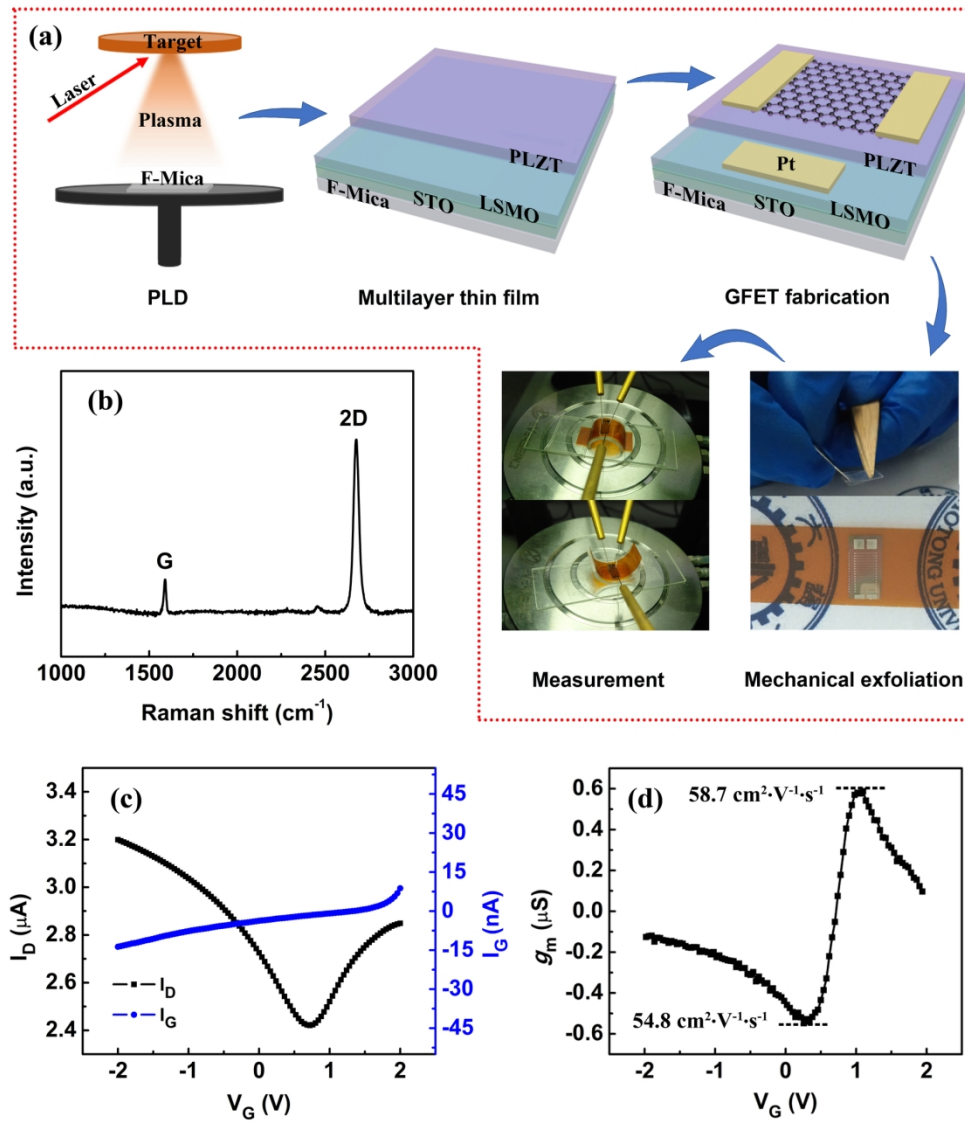
Fig. 1 (a) Fabrication process of the flexible GFET. (b) The Raman spectrum of the graphene transferred on the PLZT thin film gate. (c) The transfer characteristic of PLZT ferroelectric gate GFET, measured with a fixed drain bias V_D=10 mV. (d) The transfer conduction (g_m) of the PLZT gate GFET corresponding to the I_D-V_G curve in (c).

160x182mm (300 x 300 DPI)
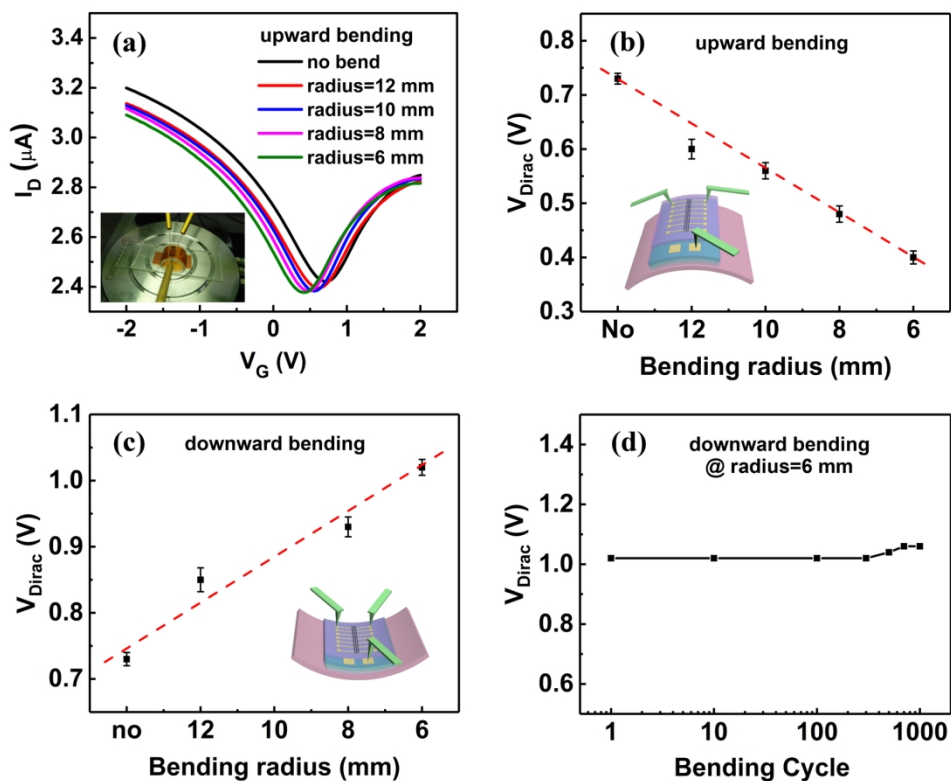
Fig. 2 (a) I_D-V_G curves measured under different upward bending state. The inset is a schematic diagram of the structure for measurement. (b) V_{Dirac} obtained from (a). The inset is the schematic diagram of the structure for measurement of transfer characteristics under upward bending state. (c) V_{Dirac} obtained under different downward bending state. The inset is the schematic diagram of the structure for measurement. (d) The V_{Dirac} as function of the cycle number obtained from the I_D-V_G characters for the flexible PLZT-gate GFET under 6 mm downward bending radius.
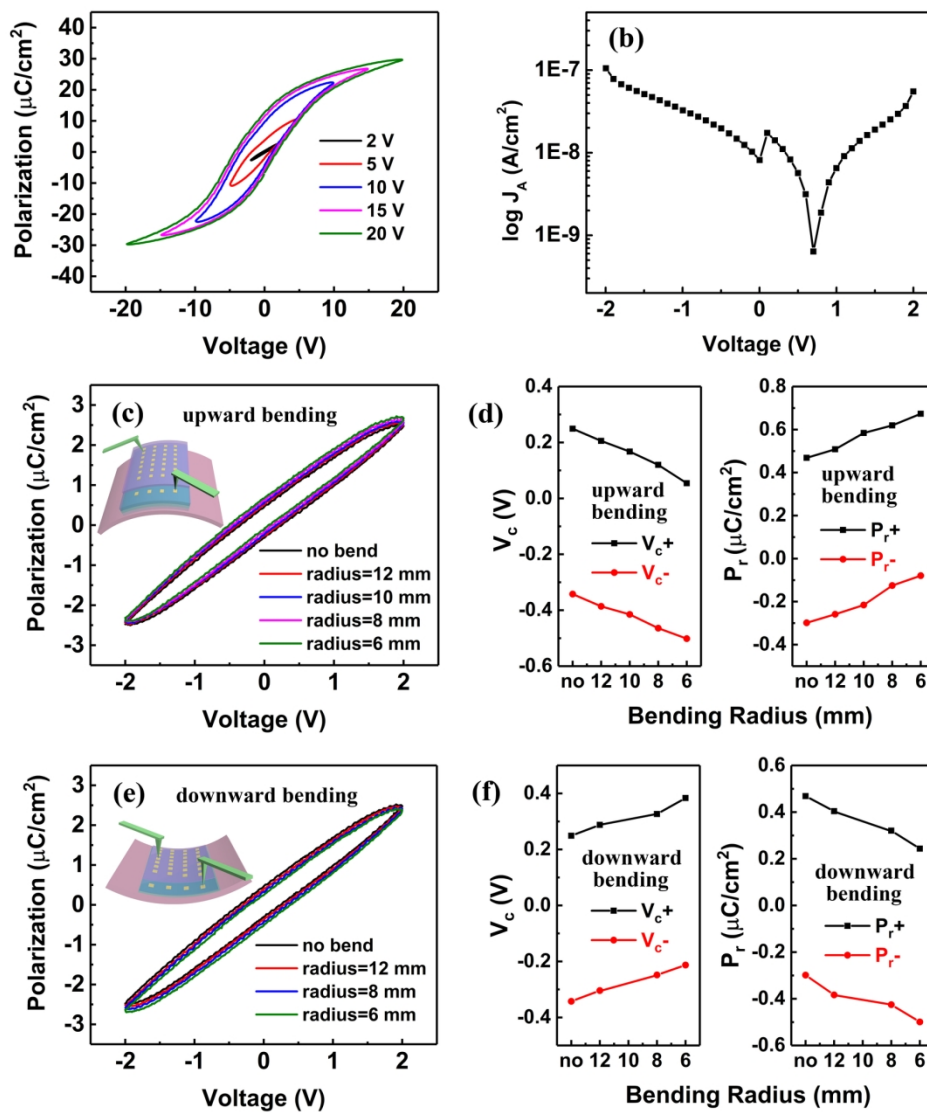
160x128mm (300 x 300 DPI)

Fig. 3 (a) Typical *P-E* loops of the PLZT thin film with LSMO bottom electrode and Pt top electrode on F-Mica. (b) Leakage current density of the sample. (c) *P-E* loops under different upward bending radii at 2 V gate voltage. The inset is schematic of the measurement. (d) V_c and P_r of the loops in (c). (e) *P-E* loops under different downward bending radii at 2 V gate voltage. The inset is schematic of the measurement. (f) V_c and P_r of the loops in (e).
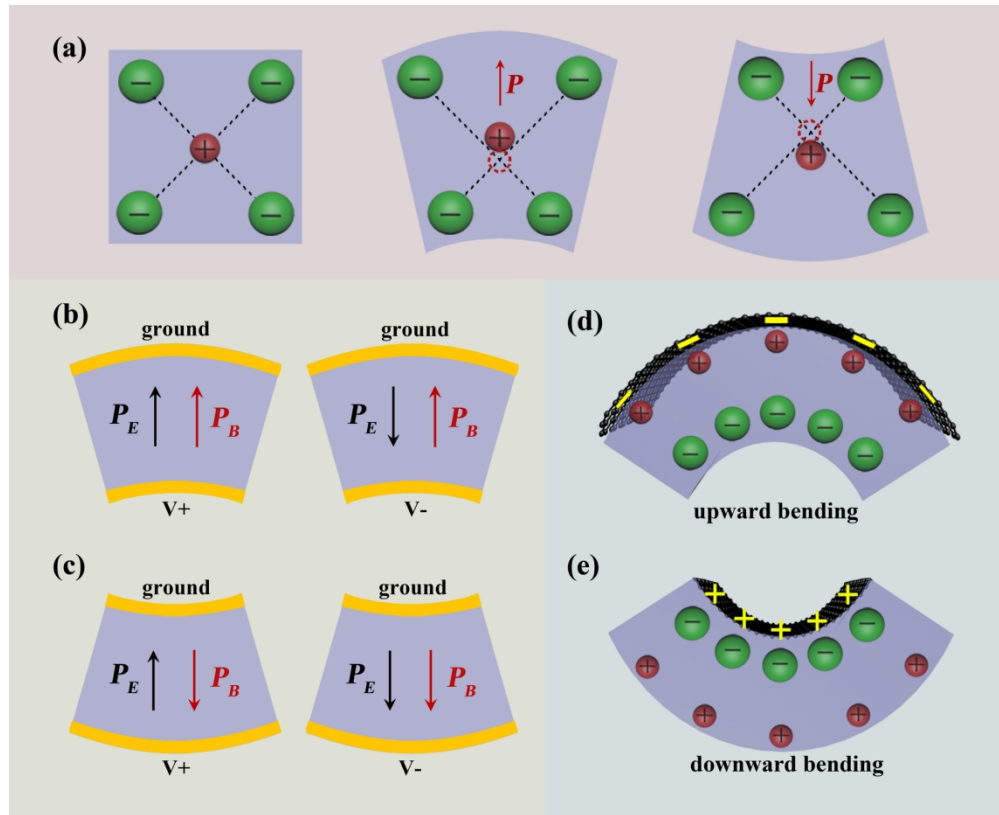
160x183mm (300 x 300 DPI)

Fig. 4 (a) Schematic diagram of the curvature-induced polarization in PLZT. (b) The polarization in PLZT when positive *V+* and negative *V-* are applied on the bottom electrode under upward bending state. (c) The polarization in PLZT when positive *V+* and negative *V-* are applied on the bottom electrode under upward bending state. (d) Negative charge doping in graphene under the upward bending state. (e) Positive charge doping in graphene under the downward bending state.

160x130mm (300 x 300 DPI)
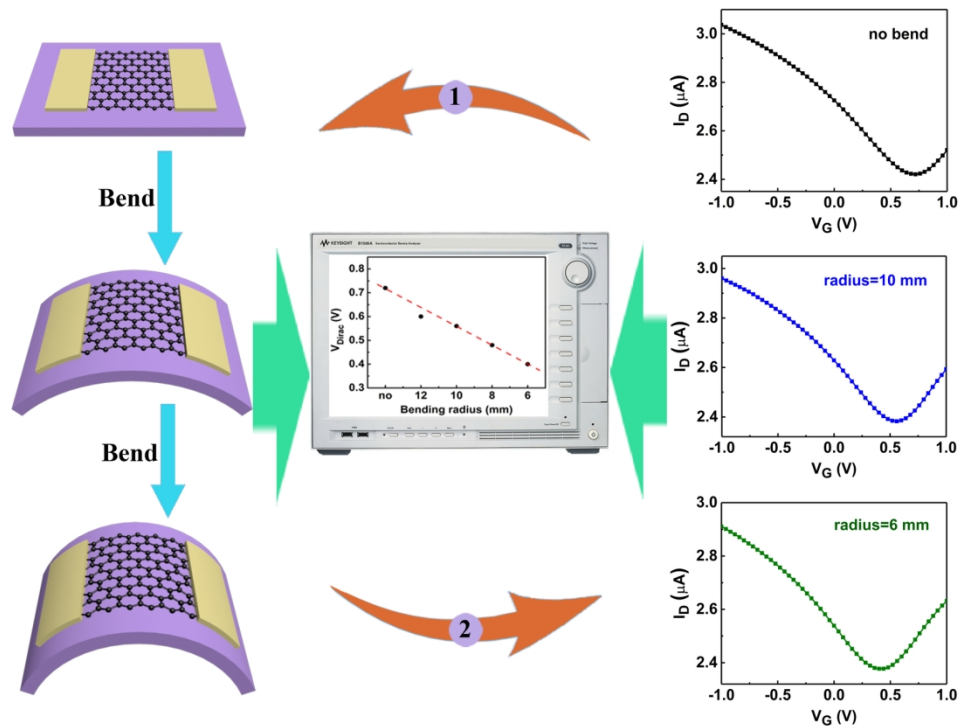
Fig. 5 Schematic illustration of the flexible mechanics-electronic sensing system for the inorganic PLZT-gated PLZT GFET.

160x145mm (300 x 300 DPI)